Journal of Sound and Vibration 326 (2009) 235–250

Contents lists available at ScienceDirect

Journal of Sound and Vibration

journal homepage: www.elsevier.com/locate/jsvi

Free vibration and lateral buckling of a cantilever slender beam with an edge crack: Experimental and numerical studies

Celalettin Karaagac [a], Hasan Öztürk [b], Mustafa Sabuncu [b,*]

[a] Mechanical Engineering Department, Ege University, Bornova, İzmir 35100, Turkey
[b] Mechanical Engineering Department, Dokuz Eylul University, Bornova, İzmir 35100, Turkey

ARTICLE INFO

Article history:
Received 20 November 2008
Received in revised form
17 March 2009
Accepted 16 April 2009
Handling Editor: C.L. Morfey
Available online 17 May 2009

ABSTRACT

The effects of crack ratios and positions on the fundamental frequencies and buckling loads of slender cantilever Euler beams with a single-edge crack are investigated both experimentally and numerically using the finite element method, based on energy approach. The governing matrix equations are derived from the standard and cracked beam elements combined with the local flexibility concept. The experiments are conducted using specimens having edge cracks of different depths at different positions to validate the numerical results obtained. The numerical results are shown to be in good agreement with the experimental results for the considered crack ratios.

1. Introduction

Beams and beamlike elements are principal constituent of many mechanical structures and used widely in high speed machinery, aircraft and lightweight structures. The lateral-torsional buckling performance of slender beams like turbine blade or aircraft wing is a limiting state that may often be a control factor in beam designs [1]. So this subject has received significant attention since Timoshenko and Gere [2] discussed it in their book, although the pioneering works were initiated in the beginning of 1900s. However, comparatively little work on lateral-torsional buckling of slender beams has been reported in the literature since then. The objective of this paper is to study the effects of crack ratio, a/h and crack location, L_1 on the lateral buckling capacity and free vibration of cantilever slender rectangular beams with an open single-edge crack, experimentally to validate the results obtained from numerical analysis and to provide information for the future researches.

In 1975, Hodges and Peters [3] quantified and modified the deficient analytical solutions for buckling loads given in the previous literature using asymptotic expansion methods. In subsequent works, the topic was dealt with analytically [1,4–7], by plotting [8], by FEM [9–11] and experimentally [12–14]. In the aforementioned studies, the beams considered are intact, that is, they do not contain any defect such as cracks. But, during operation, all structural elements are subjected to degenerative effects that may cause initiation of structural defects such as cracks which, as time progresses, lead to the catastrophic failure or breakdown of the structure [15]. So, the knowledge of the behavior of defected element is of great importance to be able to maintain the structural integrity and to generate safety parameters. As has been stated in almost all papers related to the vibration of the cracked structures, the existence of a crack reduces the local stiffness and consequently static, dynamic and stability behaviors of a structural element are altered such that these alterations may be used to detect the crack location and its size.

* Corresponding author. Tel.: +90 232 3883138/208; fax: +90 232 3887868.
E-mail address: mustafa.sabuncu@deu.edu.tr (M. Sabuncu).

0022-460X/$ - see front matter © 2009 Elsevier Ltd. All rights reserved.
doi:10.1016/j.jsv.2009.04.022

Nomenclature

a	crack depth
A	cross-sectional area of the beam
b	thickness of the beam
d	length of the finite element
d_1	crack position on the finite element
E	modulus of elasticity
f_{1c}	fundamental frequency of the cracked beam
f_{1nc}	fundamental frequency of the non-cracked beam
$F_{jn}(a/h)$	correction function
G	shear modulus
h	width of the beam
I_y, I_z	second moments of area of cross-section about y- and z-axis
I_{yz}	polar moment of inertia
J	torsional constant
$J(\alpha)$	strain energy release rate
K_{In}, K_{IIn}, K_{IIIn}	stress intensity factors for three fracture modes ($n = 1, 2,\ldots,6$)
L	length of the beam
L_1	crack location on the beam
$M(x)$	external moment about z-axis
$M_{x'}$, $M_{y'}$, $M_{z'}$	bending moments induced by buckling at any section of beam
M_{y1}, M_{y2}	lateral moments at crack section about y-axis
M_{z1}, M_{z2}	vertical moments at crack section about z-axis
P_c	critical (the lowest) buckling load of cracked beam
P_{cr}	critical (the lowest) buckling load
P_{nc}	critical (the lowest) buckling load of non-cracked beam
P_{1-6}, P_i, P_n	generalized loading ($i, n = 1, 2,\ldots,6$)
q_i	nodal displacements ($i = 1, 2,\ldots,10$)
T_1, T_2	torsional moments at crack section about x-axis
u_i	additional displacements along the direction of loading P_i
U	elastic potential energy
U_s	strain energy
$v(x)$	displacement in the direction of y-axis
V	work done by vertical tip load
$w(x)$	displacement in the direction of z-axis
x	coordinate axis along the beam length
y	coordinate axis along the beam width
z	coordinate axis along the beam thickness
α	variable along crack depth
$\gamma(x)$	rotation about x-axis
v	Poisson's ratio
ρ	mass density
σ_n	uniform remote stress at the cross-section away from crack created by generalized loading ($n = 1, 2, \ldots,6$)
c	subscript—abbreviation for the word "cracked"
cr	subscript—abbreviation for the word "critical"
i	numerator for the generalized loading and general sorting
j	numerator for the crack modes and general rowing
l	subscript—abbreviation for the word "left"
n	numerator for the generalized loading
nc	subscript—abbreviation for the word "non-cracked"
r	subscript—abbreviation for the word "right"
s	subscript—abbreviation for the word "strain"

The effects of cracks on the dynamic behaviors of beams have been the subject of many investigations. Since it is impossible to mention all of them, the reader is referred to the survey paper by Dimarogonas [16], where information and related literature can be found. In addition, several works can be mentioned as follows: Shen and Pierre [17] demonstrated a model for the prediction of the dynamic response of cracked beams and investigated the effects of a single surface crack on the free vibration of cantilever beams analytically and numerically. Eigenfrequencies of a cantilever beam with a transverse on-edge non-propagating open crack were investigated by Krawczuk and Ostachowicz [18], presenting two models of beam. Bamnios and Trochides [19] studied the influence of a transverse surface crack on the dynamic behavior of a cantilever beam both analytically and experimentally.

The vibration characteristics of a uniform Bernoulli–Euler beam with a single-edge crack were investigated by Yokoyama and Chen [20], using a modified line-spring model. Chaudhari and Maiti [21] proposed a modeling of transverse vibration of a beam with an open edge-crack, using the concept of a rotational spring to represent the crack section. A cracked beam finite element based on elasto-plastic fracture mechanics and the finite element method was formulated by Krawczuk et al. [22]. Orhan [23] studied the free and forced vibration of cantilever beam having a V-shaped edge crack, using a finite element program (Ansys).

As can be seen from the existing literature, compared to vast investigation on crack effects to dynamics of usual beams of isotropic and homogeneous or composite material, unfortunately, much less investigation on lateral-torsional buckling capacity and dynamics of cracked slender beams has been reported. To cite only one: Wang et al. [24] have investigated the coupled bending and torsional vibration of a fiber-reinforced composite cantilever slender beam with an edge crack. They have modeled the crack with a local flexibility matrix.

In the present study a finite element algorithm based on energy method is developed and experiments are carried out in order to verify the results obtained from the proposed numerical method. Matlab software is used for the numerical calculations. The local flexibility approach is adopted to model the crack, based on linear fracture mechanics and the Castigliano theorem. The Euler–Bernoulli assumptions are used in modeling the beam. The crack is assumed to be always

open and non-propagating in progress of time. It is also assumed that the crack affects only stiffness of the beam whereas the mass [18,25] and damping [25] of beam remain unchanged. As far as the authors know, both the lateral-torsional buckling capacity and free vibration of the cracked cantilever slender beam made of isotropic and homogeneous material together has not been studied prior to the work presented in this paper.

2. The local flexibility due to the crack

The cracked beam configuration considered is shown in Fig. 1. A crack on a beam introduces considerable local flexibility due to the strain energy concentration in the vicinity of the crack tip under load. The idea of an equivalent spring i.e. a local compliance is used to quantify, in a macroscopic way, the relation between the applied load and the strain concentration around the tip of the crack [26]. A beam element of rectangular cross-section has an edge crack with a tip line parallel to the z-axis i.e. with a uniform depth. A generalized loading is indicated by six general forces: an axial force P_1, shear forces P_2 and P_3, bending moments P_4 and P_5, a torsional moment P_6 [24,26] as seen in Fig. 2.

According to the Castigliano's theorem and the Paris equation, the relation between the additional displacement along the direction of loading P_i and the strain energy U_s is given by

$$u_i = \frac{\partial U_s}{\partial P_i} = \frac{\partial}{\partial P_i}\int_0^a J(\alpha)\,\mathrm{d}\alpha \tag{1}$$

where $J(\alpha) = \partial U_s/\partial\alpha$ is the strain energy release rate, a is the crack depth. Thus, the local compliance, by definition, is

$$c_{ij} = \frac{\partial u_i}{\partial P_j} = \frac{\partial^2}{\partial P_i \partial P_j}\int_0^a J(\alpha)\,\mathrm{d}\alpha \tag{2}$$

For general loading of the cracked section, the strain energy release rate $J(\alpha)$ is given [16,26–28] as

$$J(\alpha) = \frac{1}{E'}\left[\left(\sum_{n=1}^{6} K_{\mathrm{I}n}\right)^2 + \left(\sum_{n=1}^{6} K_{\mathrm{II}n}\right)^2 + (1+\nu)\left(\sum_{n=1}^{6} K_{\mathrm{III}n}\right)^2\right] \tag{3}$$

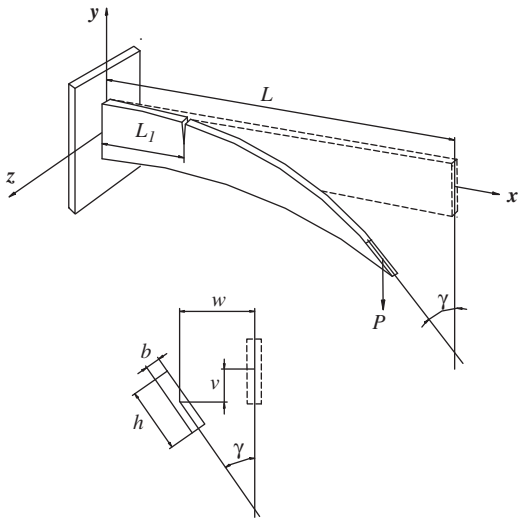

Fig. 1. Lateral buckling of a cracked cantilever beam loaded with a vertical force.

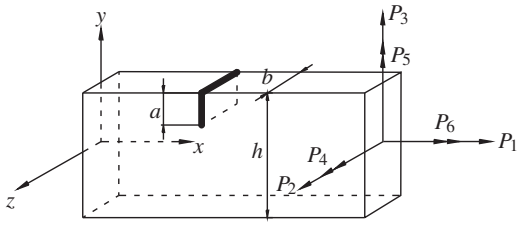

Fig. 2. Schematic view of a cracked beam under generalized loading conditions.

where $E' = E$ for plane stress, $E' = E/(1-\nu^2)$ for plane strain, $K_{\mathrm{I}n}$, $K_{\mathrm{II}n}$, $K_{\mathrm{III}n}$ are the stress intensity factors (SIFs) of the three modes of fracture (opening, sliding and tearing type) corresponding to generalized loading P_n, respectively.

To obtain results for the stress intensity factors for an edge crack on a beam, the beam is considered as an assembly of strips ordered along the z-axis as shown in Fig. 3. Hereby, the strain energy release rate $J(\alpha)$ has to be integrated along the crack width b to give [16]

$$c_{ij} = \frac{\partial u_i}{\partial P_j} = \frac{\partial^2}{\partial P_i \partial P_j} \int_{-b/2}^{b/2} \int_0^q J(\alpha)\, \mathrm{d}\alpha\, \mathrm{d}z \tag{4}$$

Substituting Eq. (3) in Eq. (4) yields the general equation for the local compliances as follows:

$$c_{ij} = \frac{\partial^2}{\partial P_i \partial P_j} \left\{ \int_{-b/2}^{b/2} \int_0^a \frac{1}{E'} \left[\left(\sum_{n=1}^{6} K_{\mathrm{I}n} \right)^2 + \left(\sum_{n=1}^{6} K_{\mathrm{II}n} \right)^2 + m \left(\sum_{n=1}^{6} K_{\mathrm{III}n} \right)^2 \right] \mathrm{d}\alpha\, \mathrm{d}z \right\} \tag{5}$$

Eq. (5) gives the components of the complete flexibility matrix of the cracked section with the expressions for the stress intensity factors which can be expressed as

$$K_{jn} = \sigma_n \sqrt{\pi a} F_{jn}(a/h), \quad j = \mathrm{I}, \mathrm{II}, \mathrm{III}, \; n = 1, 2, \ldots, 6 \tag{6}$$

where σ_n is the uniform remote stress at the cross-section away from the crack due to the n-th independent loading, a and h are the crack depth and beam width, respectively, $F_{jn}(a/h)$ represents the correction function which takes into account finite dimensions of the beam [18] and takes the form for different geometry and loading modes.

The beam can be in equilibrium in a slightly buckled form when the critical load is acting. As a result of buckling, three moments, namely $M_{x'}$, $M_{y'}$ and $M_{z'}$ are induced at any section, about a second set of coordinate axes x', y', z' that move relatively with the section as it deforms. $M_{x'}$, $M_{y'}$ and $M_{z'}$ describe twisting, lateral bending and vertical bending of the beam, respectively [11,29]. Correspondingly, the loads that the beam could take are the vertical bending (P_4), the lateral bending (P_5) and the torsional moment (P_6) as shown in Fig. 4. Thus, only the components in the flexibility matrix related to $i,j = 4,5,6$ are needed. Relating to the loadings considered, the stress intensity factors needed, given with Eq. (6), are

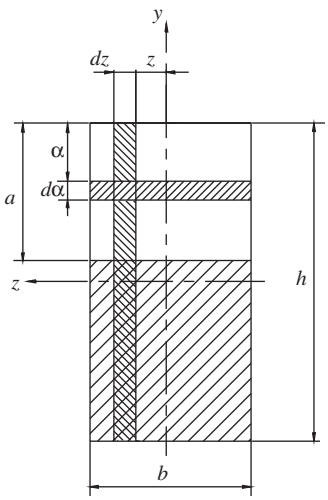

Fig. 3. Cracked section geometry.

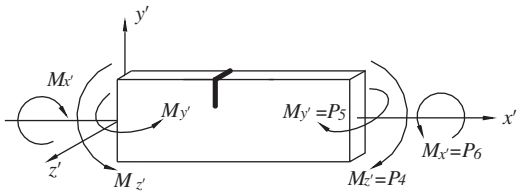

Fig. 4. Three moments present at any section during buckling.

determined [18,24] as

$$K_{I4} = \sigma_4\sqrt{\pi a}F_1(a/h), \quad \sigma_4 = \frac{6P_4}{bh^2}$$

$$K_{I5} = \sigma_5\sqrt{\pi a}F_2(a/h), \quad \sigma_5 = \frac{12P_5}{hb^3}z$$

$$K_{I1} = K_{I2} = K_{I3} = K_{I6} = 0$$

$$K_{II1} = K_{II2} = K_{II3} = K_{II4} = K_{II5} = K_{II6} = 0$$

$$K_{III6} = \sigma_6\sqrt{\pi a}F_{III}(a/h), \quad \sigma_6 = \frac{24P_6\pi^3}{\pi^5 hb^2 - 192b^3}\cos\left(\frac{\pi}{b}z\right)$$

$$K_{III1} = K_{III2} = K_{III3} = K_{III4} = K_{III5} = 0 \tag{7}$$

where

$$F_1(a/h) = \sqrt{\frac{\tan\lambda}{\lambda}}[0.923 + 0.199(1 - \sin\lambda)^4]/\cos\lambda, \quad \lambda = \frac{\pi a}{2h} \tag{7a}$$

$$F_2(a/h) = \sqrt{\frac{\tan\lambda}{\lambda}}[0.752 + 0.0.02(a/h) + 0.37(1 - \sin\lambda)^3]/\cos\lambda \tag{7b}$$

$$F_{III}(a/h) = \sqrt{\frac{\tan\lambda}{\lambda}} \tag{7c}$$

and σ_4, σ_5 denote bending stresses induced by bending, σ_6 denotes the shear stress induced by torsion along the short edge of the cross-section, determined using the classical theory of elasticity [24]. Using the SIFs in Eq. (7), Eq. (5) becomes

$$c_{ij} = \frac{\partial^2}{\partial P_i \partial P_j}\left\{\int_{-b/2}^{b/2}\int_0^a \frac{1}{E'}[(K_{I4} + K_{I5})^2 + m(K_{III6})^2]\,d\alpha\,dz\right\} \tag{8}$$

Based on Eqs. (5) and (8), the final local flexibility matrix with the components of interest can be formed as

$$\mathbf{c_{ij}} = \begin{bmatrix} c_{44} & 0 & 0 \\ 0 & c_{55} & 0 \\ 0 & 0 & c_{66} \end{bmatrix} \tag{9}$$

3. The finite element model

A finite element model is developed to represent a cracked beam element of length d and the crack is located at a distance d_1 from the left end of the element as shown in Fig. 5. The element is then considered to be split into two segments by the crack. The left and right segments are represented by non-cracked subelements. The crack represents net ligament

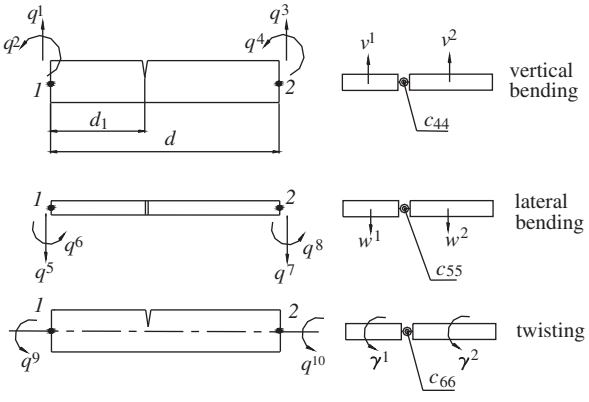

Fig. 5. The cracked beam finite element.

effect created by loadings. This effect can be related to the deformation of the net ligament through the compliance expressions (c_{ij}) by replacing the net ligament with a fictitious spring connecting both faces of the crack [20]. So, the spring effects are introduced to the system by using the local flexibility matrix given by Eq. (9). The cracked or non-cracked element has two nodes with five degrees of freedom in each node. They are denoted as vertical bending displacements (v_1, v_2), lateral bending displacements (w_1, w_2), slopes (v_1', v_2', w_1', w_2') and rotations about x-axis (γ_1, γ_2), where prime ($'$) denotes differentiation with respect to the longitudinal coordinate x.

The displacements $v(x), w(x)$ due to vertical and lateral bending are approximated by cubic polynomials [11,17,22,26], while the rotation $\gamma(x)$ can be expressed by linear functions, for the left and right segments of the element.

for $0 \leqslant x \leqslant d_1$,

$$v_1(x) = a_1 + a_2 x + a_3 x^2 + a_4 x^3$$

$$w_1(x) = b_1 + b_2 x + b_3 x^2 + b_4 x^3$$

$$\gamma_1(x) = c_1 + c_2 x \tag{10a}$$

for $d_1 \leqslant x \leqslant d$,

$$v_2(x) = a_5 + a_6 x + a_7 x^2 + a_8 x^3$$

$$w_2(x) = b_5 + b_6 x + b_7 x^2 + b_8 x^3$$

$$\gamma_2(x) = c_3 + c_4 x \tag{10b}$$

The coefficients a_{1-8}, b_{1-8}, c_{1-4} of the polynomials can be expressed uniquely in terms of the boundary conditions shown in Fig. 5 and the local flexibility concept at the crack location. Eventually the following expressions are obtained for a cracked element:

Vertical bending:

$$v_1(0) = q_1, \quad v_1'(0) = q_2$$

$$v_2(d) = q_3, \quad v_2'(d) = q_4 \tag{11a}$$

Lateral bending:

$$w_1(0) = q_5, \quad w_1'(0) = q_6$$

$$w_2(d) = q_7, \quad w_2'(d) = q_8 \tag{11b}$$

Twisting about x-axis:

$$\gamma_1(0) = q_9, \quad \gamma_2(d) = q_{10} \tag{11c}$$

At the crack location d_1, the flexibility concept requires:

Vertical bending:

(a) Continuity of the vertical displacement

$$v_1(d_1) = v_2(d_1) \tag{12a}$$

(b) Discontinuity of the cross-sectional rotation

$$v_2'(d_1) = v_1'(d_1) + c_{44} M_{z1}(d_1) \tag{12b}$$

where $M_{z1}(d_1) = EI_z v_1''|_{x=d_1}$.

(c) Continuity of the vertical bending moment

$$M_{z1}(d_1) = M_{z2}(d_1) \tag{12c}$$

(d) Continuity of the shear force

$$S_{y1}(d_1) = S_{y2}(d_1) \tag{12d}$$

Lateral bending:

(e) Continuity of the lateral displacement

$$w_1(d_1) = w_2(d_1) \tag{13a}$$

(f) Discontinuity of the cross-sectional rotation

$$w_2'(d_1) = w_1'(d_1) + c_{55}M_{y1}(d_1) \tag{13b}$$

where $M_{y1}(d_1) = EI_y w_1''|_{x=d_1}$.

(g) Continuity of the lateral bending moment

$$M_{y1}(d_1) = M_{y2}(d_1) \tag{13c}$$

(h) Continuity of the shear force

$$S_{z1}(d_1) = S_{z2}(d_1) \tag{13d}$$

Twisting about x-axis:

(i) Discontinuity of the torsional angle

$$\gamma_2(d_1) = \gamma_1(d_1) + c_{66}T_1(d_1) \tag{14a}$$

where $T_1(d_1) = GJ\gamma_1'|_{x=d_1}$.

(j) Continuity of the torsional moment

$$T_1(d_1) = T_2(d_1) \tag{14b}$$

By considering Eq. (10) describing the displacements for the left and right part of the element and rearranging Eqs. (11)–(14), the nodal displacements can be expressed in matrix forms as

$$\mathbf{q_v} = \mathbf{D_v a}, \quad \mathbf{q_w} = \mathbf{D_w b}, \quad \mathbf{q_\gamma} = \mathbf{D_\gamma c} \tag{15}$$

where

$$\mathbf{q_v} = [q_1 \;\; q_2 \;\; 0 \;\; 0 \;\; 0 \;\; 0 \;\; q_3 \;\; q_4]^{\mathrm{T}}$$

$$\mathbf{q_w} = [q_5 \;\; q_6 \;\; 0 \;\; 0 \;\; 0 \;\; 0 \;\; q_7 \;\; q_8]^{\mathrm{T}}$$

$$\mathbf{q_\gamma} = [q_9 \;\; 0 \;\; 0 \;\; q_{10}]^{\mathrm{T}} \tag{15a}$$

$$\mathbf{a} = [a_1 \;\; a_2 \;\; a_3 \;\; a_4 \;\; a_5 \;\; a_6 \;\; a_7 \;\; a_8]^{\mathrm{T}}$$

$$\mathbf{b} = [b_1 \;\; b_2 \;\; b_3 \;\; b_4 \;\; b_5 \;\; b_6 \;\; b_7 \;\; b_8]^{\mathrm{T}}$$

$$\mathbf{c} = [c_1 \;\; c_2 \;\; c_3 \;\; c_4]^{\mathrm{T}} \tag{15b}$$

and $\mathbf{D_v}$, $\mathbf{D_w}$, $\mathbf{D_\gamma}$ matrices are given by Eq. (A.1) in Appendix.

Matrices in Eq. (15) can be written in compact form as

$$\begin{Bmatrix} \mathbf{q_v} \\ \mathbf{q_w} \\ \mathbf{q_\gamma} \end{Bmatrix}_{20\times1} = \mathbf{D}_{20\times20} \begin{Bmatrix} \mathbf{a} \\ \mathbf{b} \\ \mathbf{c} \end{Bmatrix}_{20\times1} \tag{16}$$

Taking the inverse of Eq. (16), the matrix giving the constants a_{1-8}, b_{1-8}, c_{1-4} is obtained as

$$\begin{Bmatrix} \mathbf{a} \\ \mathbf{b} \\ \mathbf{c} \end{Bmatrix}_{20\times1} = \mathbf{C}_{120\times20} \begin{Bmatrix} \mathbf{q_v} \\ \mathbf{q_w} \\ \mathbf{q_\gamma} \end{Bmatrix}_{20\times1} \tag{17}$$

where $\mathbf{C}_1 = \mathbf{D}^{-1}$. Using Eq. (17), the expressions relating the constants to the nodal displacements can be presented as follows:

$$a_1 = C_{11}q_1 + C_{12}q_2 + C_{17}q_3 + C_{18}q_4 + C_{19}q_5 + C_{110}q_6 + C_{115}q_7 + C_{116}q_8 + C_{117}q_9 + C_{120}q_{10}$$

$$a_2 = C_{21}q_1 + C_{22}q_2 + C_{27}q_3 + C_{28}q_4 + C_{29}q_5 + C_{210}q_6 + C_{215}q_7 + C_{216}q_8 + C_{217}q_9 + C_{220}q_{10}$$

$$\vdots$$

$$b_1 = C_{91}q_1 + C_{92}q_2 + C_{97}q_3 + C_{98}q_4 + C_{99}q_5 + C_{910}q_6 + C_{915}q_7 + C_{916}q_8 + C_{917}q_9 + C_{920}q_{10}$$

$$\vdots$$

$$c_1 = C_{171}q_1 + C_{172}q_2 + C_{177}q_3 + C_{178}q_4 + C_{179}q_5 + C_{1710}q_6 + C_{1715}q_7 + C_{1716}q_8 + C_{1717}q_9 + C_{1720}q_{10}$$

$$\vdots \tag{18}$$

or in matrix form

$$\left\{\begin{array}{c}\mathbf{a}\\ \mathbf{b}\\ \mathbf{c}\end{array}\right\}_{20\times1}=\mathbf{C}_{20\times10}\left\{\begin{array}{c}\mathbf{q_v}\\ \mathbf{q_w}\\ \mathbf{q_\gamma}\end{array}\right\}_{10\times1} \tag{19}$$

Thus, substituting Eq. (19) into Eqs. (10a) and (10b), the displacements at any point of the element are obtained in matrix form:

for $0\leqslant x\leqslant d_1$

$$\mathbf{v}_1=\mathbf{P}\mathbf{a}_1,\quad \mathbf{w}_1=\mathbf{P}\mathbf{b}_1,\quad \gamma_1=\mathbf{R}\mathbf{c}_1 \tag{20a}$$

for $d_1\leqslant x\leqslant d$

$$\mathbf{v}_2=\mathbf{P}\mathbf{a}_2,\quad \mathbf{w}_2=\mathbf{P}\mathbf{b}_2,\quad \gamma_2=\mathbf{R}\mathbf{c}_2 \tag{20b}$$

in which the matrices $\mathbf{a}_1,\mathbf{b}_1,\mathbf{c}_1,\mathbf{a}_2,\mathbf{b}_2,\mathbf{c}_2,\mathbf{P}$ and $\mathbf{R}$ are given by Eq. (A.2) in Appendix. So, the generalized displacement vector can be expressed as

$$\mathbf{q_e}=[q_1\ \ q_2\ \ q_5\ \ q_6\ \ q_9\ \ q_3\ \ q_4\ \ q_7\ \ q_8\ \ q_{10}]^{\mathrm{T}} \tag{21}$$

4. Energy equations

Energy equations should be expressed separately for the cracked element and intact elements on the left and right side of the cracked element. The elastic potential energy U, with the warping and shear effects neglected, due to vertical and lateral bendings and twisting, of an Euler beam with an elemental length d is given [2,11,27,30,31]:

for the intact elements on the left side of the cracked element:

$$U_l=\frac{1}{2}\left(\int_0^d EI_z(v_1'')^2\,\mathrm{d}x\right)+\frac{1}{2}\left(\int_0^d EI_y(w_1'')^2\,\mathrm{d}x\right)+\frac{1}{2}\left(\int_0^d GJ(\gamma_1')^2\,\mathrm{d}x\right) \tag{22a}$$

for the cracked element:

$$\begin{aligned}U_c=&\frac{1}{2}\left(\int_0^{d_1} EI_z(v_1'')^2\,\mathrm{d}x\right)+\frac{1}{2}\left(\int_0^{d_1} EI_y(w_1'')^2\,\mathrm{d}x\right)+\frac{1}{2}\left(\int_0^{d_1} GJ(\gamma_1')^2\,\mathrm{d}x\right)\\&+\frac{1}{2}\left(\int_{d_1}^{d} EI_z(v_2'')^2\,\mathrm{d}x\right)+\frac{1}{2}\left(\int_{d_1}^{d} EI_y(w_2'')^2\,\mathrm{d}x\right)+\frac{1}{2}\left(\int_{d_1}^{d} GJ(\gamma_2')^2\,\mathrm{d}x\right)\end{aligned} \tag{22b}$$

for the intact elements on the right side of the cracked element:

$$U_r=\frac{1}{2}\left(\int_0^d EI_z(v_2'')^2\,\mathrm{d}x\right)+\frac{1}{2}\left(\int_0^d EI_y(w_2'')^2\,\mathrm{d}x\right)+\frac{1}{2}\left(\int_0^d GJ(\gamma_2')^2\,\mathrm{d}x\right) \tag{22c}$$

Similarly, the kinetic energy T of an element in length d of an Euler beam is given as:

for the intact elements on the left side of the cracked element:

$$T_l=\frac{1}{2}\rho\left[\int_0^d A(\dot{v}_1^2+\dot{w}_1^2+I_{yz}\dot{\gamma}_1^2)\,\mathrm{d}x\right] \tag{23a}$$

for the cracked element:

$$T_c=\frac{1}{2}\rho\left[\int_0^{d_1} A(\dot{v}_1^2+\dot{w}_1^2+I_{yz}\dot{\gamma}_1^2)\,\mathrm{d}x\right]+\frac{1}{2}\rho\left[\int_{d_1}^{d} A(\dot{v}_2^2+\dot{w}_2^2+I_{yz}\dot{\gamma}_2^2)\,\mathrm{d}x\right] \tag{23b}$$

for the intact elements on the right side of the cracked element:

$$T_r=\frac{1}{2}\rho\left[\int_0^d A(\dot{v}_2^2+\dot{w}_2^2+I_{yz}\dot{\gamma}_2^2)\,\mathrm{d}x\right] \tag{23c}$$

in which the first, second and third terms represent the energies due to vertical, lateral and twisting motions, respectively.

The work done V by the vertical displacement of a tip load P as the beam buckles is given [11,13,14]:

for the intact elements on the left side of the cracked element:

$$V_l=\int_0^d M(x)\gamma_1(w_1'')\,\mathrm{d}x \tag{24a}$$

for the cracked element:

$$V_c = \int_0^{d_1} M(x)\gamma_1(w_1'')\,dx + \int_{d_1}^{d} M(x)\gamma_2(w_2'')\,dx \tag{24b}$$

for the intact elements on the right side of the cracked element:

$$V_r = \int_0^{d} M(x)\gamma_2(w_2'')\,dx \tag{24c}$$

where $M(x) = P(L - x)$.

5. Equation of motion

By substituting the expressions of Eq. (20) into the energy equations. (22)–(24), the elastic stiffness matrix $\mathbf{k_e}$, geometrical stiffness matrix $\mathbf{k_g}$ and mass matrix $\mathbf{m_e}$ are obtained for both cracked finite element and intact finite elements. Mass and stiffness matrices of each beam element are used to form global mass and stiffness matrices. By performing the required operations for the entire system, one obtains the following governing matrix equations giving natural frequency and critical buckling load, respectively:

$$(\mathbf{K} - f^2\mathbf{M})\mathbf{q} = 0 \tag{25a}$$

$$(\mathbf{K} - \mathbf{P}_{cr}\mathbf{K}_g)\mathbf{q} = 0 \tag{25b}$$

where $\mathbf{K}, \mathbf{K_g}$ and $\mathbf{M}$ represent global elastic stiffness, geometrical stiffness and mass matrices, respectively.

6. Detail of test specimens

Shanmugam and Thevendran [14] state that large-scale model tests, although desirable for proper representation of the behavior of a prototype, are expensive and time consuming. The amount of test data that could be obtained would, therefore, be limited. Use of small-scale models to simulate the behavior of large scale structures would be advantageous. Following their advice, in this study, small-scale beam models made of carbon-steel sheet are used. The specimens have a length of 350 mm (span length $L = 250$ mm plus support length 100 mm), thickness $b = 1$ mm and width $h = 25$ mm. They are laser cut from carbon-steel sheet carefully to the required dimensions. Cracks are simulated by very thin slots with a width of 0.2 mm which are also made by laser cut. The cracked test specimens are grouped under 10 categories to study the effect of crack position and crack ratio. Grouping is made according to, essentially, predetermined crack position, namely $L_1 = 0.0L$, $L_1 = 0.1L$, etc., up to $L_1 = 0.9L$. There are five edge cracked beams with a crack ratio (a/h) ranging from 0.1 to 0.5 in each group. In addition to 45 cracked beams, extra two beams without any crack are prepared to determine the buckling load and free vibration. Thus, the considered crack positions and crack lengths are $L_1 = 0, 25, 50, 75, 100, 125, 150, 175, 200, 225$ mm, $a = 2.5, 5, 7.5, 10, 12.5$ mm.

In the works referenced here crack ratio was generally considered up to 0.6, except the works of Shen and Pierre [17], Orhan [23], Fernandez-Saez et al. [31] and Gudmundson [32]. This consideration may be due to the fact that the expressions (7a) and (7b) are valid for crack ratios up to 0.6 [20] and to extend the investigation for crack ratios larger than 0.6 was found impractical [28]. In the present study, numerical analyses and experiments are performed considering the crack ratios up to 0.5.

7. Experimental procedures

The test fixture needed has to be robust and stabile to test the specimens under loading. Two angles fitted to a steel-frame are used to clamp the specimens securely by bolting so that the fix-end condition is properly ensured. The experimental program is implemented in two stages. The specimens are tested to ascertain the fundamental frequencies in first stage and the buckling loads in second stage. Experimental procedure is the same for all specimens. Each of 47 specimens is adjusted horizontally by bubble level and fixed by steel angles in turn and is tested at the span of 250 mm for, firstly, the free vibration and for, secondly, the buckling load.

The experimental set-up for free vibration is shown schematically in Fig. 6a. A miniature transducer is used to measure frequency of the lateral vibration and is mounted on a place which is as close as possible to the fix-end to diminish the effect of transducer mass added to that of specimen on vibration. Signal conditioning and integration are carried out in related hardware. LabView 7 software is used for data acquisition and storage, display and assessment of spectra. Vibration measurements are made by applying an impulse to the specimen and letting it vibrate freely.

The specimens are tested under single point loading acting at the centroid of the free end cross-section. For this, a hole of 2 mm diameter, which is very close to the free end, is made to provide a bearing for a diamond shaped arrangement used to suspend the weight hanger vertically below the centroid of the free end (Fig. 6b). The purpose of the diamond shaped arrangement is to ensure the rotation of the side of the beam without touching the hooked end of the weight hanger during

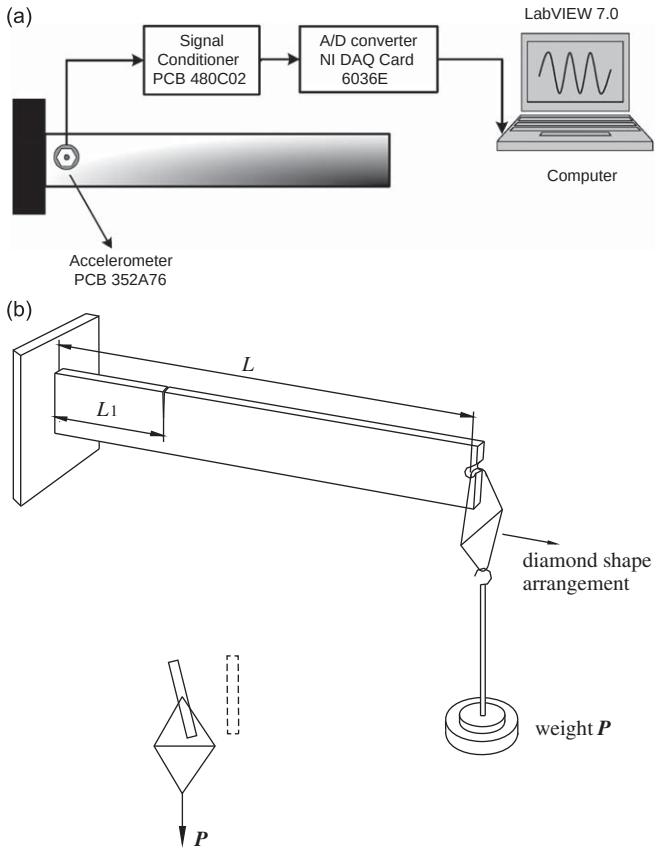

Fig. 6. (a) The experimental set-up for free vibration measuring. (b) Schematic layout of the lateral buckling test rig.

lateral buckling. The hooked end of the weight hanger is suspended from the bottom corner of the diamond shaped arrangement to ensure that the line of action of the weights always passes vertically through the centroid of the free end cross-section. Lateral stops at selected locations along the span length are provided in order to avoid excessive lateral deflections which may lead to failure of the specimens. Load is applied in increments by adding weights each time to the hanger, starting from zero. Smaller incremental weights are used as the applied load approaches the critical load. The buckling load is obtained by weighing the total weight under which the specimen makes instantaneous excessive lateral deflection.

8. Results and discussions

To verify the reliability (accuracy) and validity of the present finite element model, the fundamental frequencies and the critical (the lowest) buckling loads for 45 beams with edge cracks of different lengths at different positions and for two beams without crack have been experimentally examined. In the finite element analysis using Matlab software, the numerical results have been also obtained for the experimentally investigated beams having same crack lengths and crack positions. In the numerical analyses, the beam is discretized with 11 finite elements and the material properties have been taken as $E = 184.21$ GPa, $G = 70.85$ GPa,$v = 0.3$, $\rho = 7810$ kg/m^3.

8.1. Frequency experiments

The experimental results along with the corresponding numerical results and differences between them are given in Table 1. The results related to non-cracked beams are also included in Table 1. In addition to the Table 1, Figs. 7(a–k) show the effect of the crack ratio a/h on the fundamental frequencies of the cracked beams having different crack positions. Each plot, basically, contains two curves showing experimental and numerical results. Curve for the experimental results is presented by the best-fit line through the data points. The fundamental frequencies f_{1c} of cracked beams obtained from

Table 1
Fundamental frequencies obtained experimentally and numerically for cracked and non-cracked beams.

Fundamental frequency, f_{1c} (Hz)									
L_1/L	0.0			0.1			0.2		
a/h	Exp.	FEM	Diff. (%)	Exp.	FEM	Diff. (%)	Exp.	FEM	Diff. (%)
0.1	12.324	12.535	1.72	12.298	12.536	1.93	12.352	12.536	1.49
0.2	12.126	12.472	2.85	12.224	12.474	2.05	12.275	12.477	1.64
0.3	12.023	12.325	2.51	12.145	12.333	1.55	12.152	12.342	1.56
0.4	11.925	12.006	0.68	11.953	12.030	0.65	12.028	12.054	0.22
0.5	11.627	11.316	−2.67	11.797	11.384	−3.50	11.822	11.450	−3.15
L_1/L	0.3			0.4			0.5		
a/h	Exp.	FEM	Diff. (%)	Exp.	FEM	Diff. (%)	Exp.	FEM	Diff. (%)
0.1	12.348	12.537	1.53	12.327	12.537	1.70	12.376	12.538	1.30
0.2	12.275	12.480	1.67	12.277	12.482	1.67	12.376	12.485	0.88
0.3	12.203	12.355	1.24	12.227	12.357	1.06	12.327	12.364	0.30
0.4	12.101	12.075	−0.21	12.152	12.094	−0.48	12.302	12.110	−1.56
0.5	12.002	11.505	−4.14	12.102	11.550	−4.56	12.302	11.586	−5.82
L_1/L	0.6			0.7			0.8		
a/h	Exp.	FEM	Diff. (%)	Exp.	FEM	Diff. (%)	Exp.	FEM	Diff. (%)
0.1	12.398	12.538	1.13	12.473	12.539	0.53	12.475	12.539	0.52
0.2	12.375	12.487	0.91	12.426	12.490	0.52	12.429	12.492	0.51
0.3	12.375	12.371	−0.03	12.402	12.377	−0.20	12.405	12.382	−0.18
0.4	12.326	12.124	−1.64	12.376	12.137	−1.94	12.375	12.147	−1.84
0.5	12.252	11.613	−5.21	12.376	11.632	−6.02	12.375	11.643	−5.92
L_1/L	0.9			Non-cracked (f_{1nc})					
a/h	Exp.	FEM	Diff. (%)	Exp.	FEM	Diff. (%)			
0.0	–	–	–	12.527	12.555	0.22			
0.1	12.501	12.540	0.31						
0.2	12.452	12.494	0.34						
0.3	12.426	12.387	−0.32						
0.4	12.405	12.156	−2.00						
0.5	12.376	11.648	−5.89						

both numerical solutions and experiments are normalized by the fundamental frequency f_{1nc} of the non-cracked beam obtained from experiments. It is obvious from both Table 1 and plots that a good agreement is observed between the results up to the crack ratio $a/h = 0.5$ for all crack positions. But, as two curves progress together along the abscissa, the curve of numerical results branches off down just after the crack ratio $a/h = 0.3$ depending on the crack positions and makes difference with the curve of experiments. But, the difference does not exceed 6%. This case may be due to the fact that the expressions (7a)–(7b) have a maximum error of 0.5% for all crack lengths [32] and the flexibility coefficients, which are functions of crack ratio and go infinity with a/h approaching unity, may not be able to describe the vibration characteristics for crack ratios closing to unity [24]. It is obvious from the figures that, each curve, shifting up, approaches the curve ($f_{1c}/f_{1nc} = 1$) of non-cracked beam as the crack location L_1 moves towards the free end of beam and, at last, coincides well with the curve of non-cracked beam for the crack locations higher than$L_1 = 0.5L$. This phenomenon can be explained as; the drop in frequency is greater for crack positions close to the clamped end while the frequency is almost unchanged when the crack is located close to the free end. In other words, the frequency drop is the greatest for a crack position located where the bending moment is the largest [17].

8.2. Buckling load experiments

For each beam tested, the buckling load is predicted using numerical analysis. The experimental results along with the corresponding numerical results are given in Table 2 to be able to show the differences between them and plotted in Figs. 8(a–k) as functions of crack ratios. Again, the results related to the non-cracked beams are included in Table 2 and the critical (lowest) loads P_c of cracked beams obtained from both numerical solution and experiments are normalized by the critical (lowest) load P_{nc} of the non-cracked beam obtained from experiments. The plots are similar to those plotted for

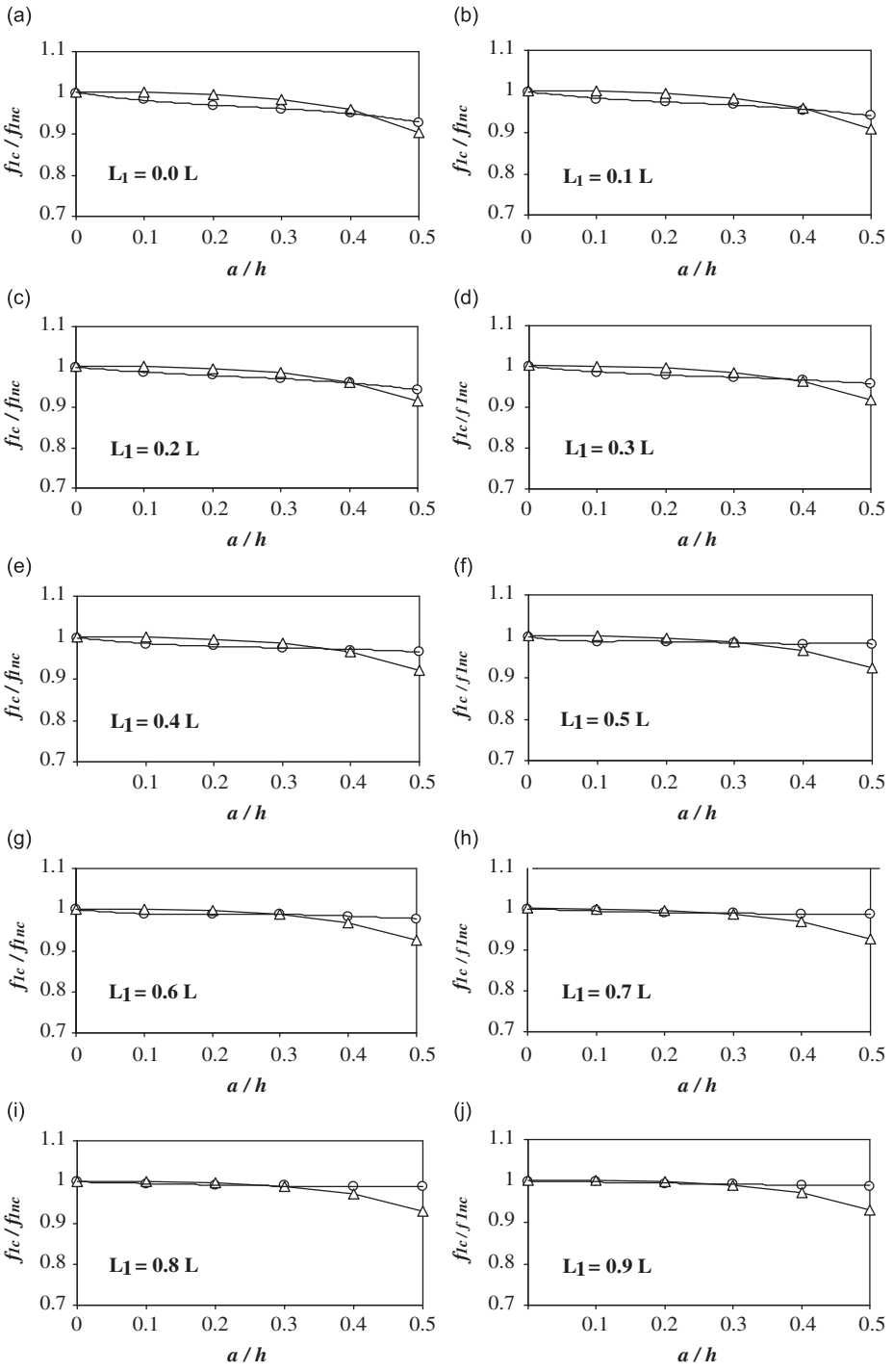

Fig. 7. Variation of natural frequency versus crack ratio at different crack positions, —○—: experimental; —Δ—: numerical results.

fundamental frequencies, so similar observations can be made for buckling loads. The only difference is that the experimental data are lower than the numerical results and the discrepancies between the curves for crack ratio higher than $a/h = 0.2$ are remarkable. This is due to the facts that specimens may have initial imperfections, which may play important role on decreasing the buckling load, and exhibit little lateral post buckling stiffness especially for the crack positions where the crack is close to the clamped end. An interesting feature pertaining to the curves is that as the crack

Table 2
Critical (lowest) buckling loads obtained experimentally and numerically for cracked and non-cracked beams.

Critical load, P_c (N)									
L_1/L	0.0			0.1			0.2		
a/h	Exp.	FEM	Diff. (%)	Exp.	FEM	Diff. (%)	Exp.	FEM	Diff. (%)
0.1	30.127	30.027	−0.33	30.166	30.140	−0.08	30.244	30.293	0.16
0.2	28.302	29.290	3.49	29.283	29.542	0.88	29.342	29.873	1.81
0.3	27.968	28.382	1.48	29.077	28.791	−0.98	29.204	29.331	0.43
0.4	24.005	27.258	13.55	26.036	27.855	6.98	26.301	28.626	8.84
0.5	22.386	25.844	15.44	23.348	26.659	14.18	24.172	27.702	14.60
L_1/L	0.3			0.4			0.5		
a/h	Exp.	FEM	Diff. (%)	Exp.	FEM	Diff. (%)	Exp.	FEM	Diff. (%)
0.1	30.313	30.432	0.39	30.342	30.524	0.60	30.352	30.579	0.75
0.2	29.656	30.171	1.73	29.714	30.377	2.23	29.783	30.496	2.39
0.3	29.263	29.824	1.91	29.459	30.174	2.42	29.548	30.373	2.79
0.4	27.223	29.356	7.83	28.027	29.892	6.65	28.851	30.205	4.69
0.5	25.790	28.716	11.34	26.565	29.494	11.03	28.057	29.966	6.81
L_1/L	0.6			0.7			0.8		
a/h	Exp.	FEM	Diff. (%)	Exp.	FEM	Diff. (%)	Exp.	FEM	Diff. (%)
0.1	30.362	30.598	0.77	30.470	30.611	0.46	30.509	30.611	0.33
0.2	29.783	30.548	2.56	30.352	30.568	0.71	30.431	30.572	0.46
0.3	29.607	30.466	2.90	30.283	30.500	0.71	30.421	30.504	0.27
0.4	29.057	30.348	4.44	29.989	30.397	1.36	30.127	30.408	0.93
0.5	28.822	30.181	4.71	29.626	30.259	2.13	29.979	30.276	0.99
L_1/L	0.9			Non-cracked. (P_{nc})					
a/h	Exp.	FEM	Diff. (%)	Exp.	FEM	Diff. (%)			
0.0	–	–	–	30.650	30.625	−0.08			
0.1	30.509	30.609	0.33						
0.2	30.597	30.574	−0.08						
0.3	30.607	30.507	−0.33						
0.4	30.617	30.411	−0.67						
0.5	30.764	30.278	−1.58						

position moves towards the free end, each curve, shifting up, approaches the curve ($P_c/P_{nc} = 1$)of non-cracked beam and they coincide well for the crack positions starting from $L_1 = 0.7L$. Significant reduction in the buckling capacity, in comparison with the capacity of the corresponding beams with no crack, can be seen in many cases. It is clear from figures that reduction in the buckling capacity is higher when the crack locates near the clamped end of beam. However, this reduction becomes less as crack position L_1 is moved towards the free end and almost negligible when the crack is positioned very close to the free end. This means that maximum reduction in buckling load occurs at sections subjected to large bending moments [14].

9. Conclusions

In this study, the effects of crack ratio and crack positions on the fundamental frequencies and the critical (the lowest) buckling loads of cracked cantilever beams have been investigated numerically and experimentally. A total of 94 both fundamental frequency and buckling load experiments have been conducted on the cracked and non-cracked specimens to ensure the validity of the finite element model developed. Plots of fundamental frequencies and buckling loads versus crack ratios for different crack positions show good correlation when comparing experimental and numerical results. In most cases experimental results differ within 6% for frequency and 10% for buckling load from the corresponding numerical results, so numerical analysis based on energy method can predict fairly accurate fundamental frequencies and buckling loads of considered beams. Results also show that the presence of cracks can reduce both fundamental frequency and buckling load depending on crack ratio and crack position as concluded in many paper referred here. For small crack ratios, the reductions in fundamental frequency and buckling load are small, becoming progressively greater at larger crack ratios. The higher drops in fundamental frequency and buckling load are observed when the crack locates near the clamped end.

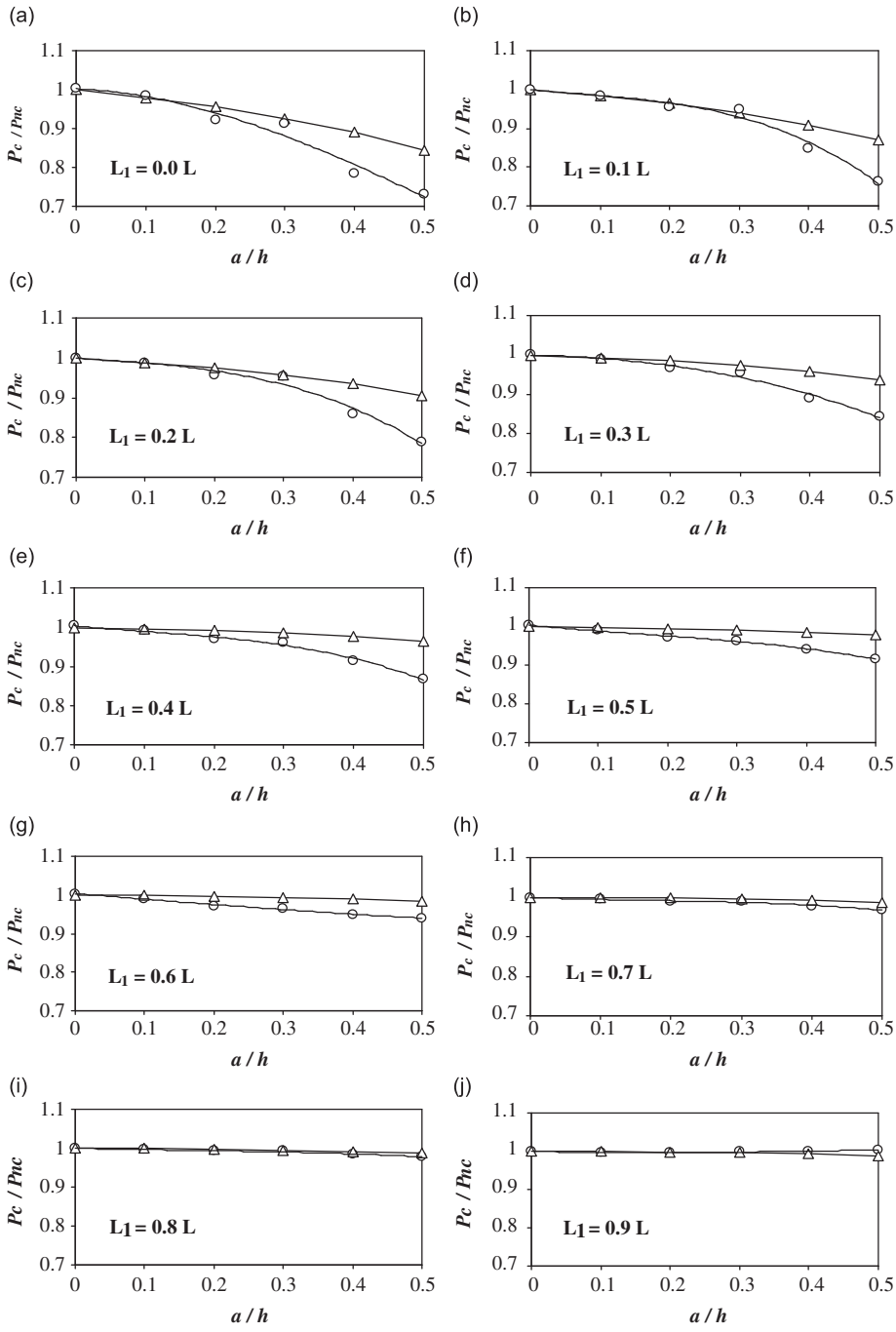

Fig. 8. Variation of buckling loads versus crack ratio with different crack positions, —○—: experimental; —Δ—: numerical results.

Thus, it is concluded that once the position of crack is fixed, the relative size of crack may be estimated with acceptable accuracy using the plots to be drawn, showing the changes in natural frequency versus crack ratios and corresponding mode shapes.

The numerical method presented in this paper is straightforward one involving no tedious mathematics and polynomial approximation for the displacements has given results with reasonable accuracy. Consequently, the numerical method offered, of course, applicable easily to the particular cases of structural elements with single or multiple cracks, having various geometry and boundary conditions provided that the necessary stress intensity factors are known.

Appendix A

$$\mathbf{D_v}=\begin{bmatrix}1&0&0&0&0&0&0&0\\0&1&0&0&0&0&0&0\\0&0&1&0&0&0&-1&0\\0&0&0&1&0&0&0&-1\\-1&0&S1&S2&1&0&0&0\\0&-1&S3&S4&0&1&0&0\\0&0&0&0&1&d&d^2&d^3\\0&0&0&0&0&1&2d&3d^2\end{bmatrix},\quad \mathbf{D_w}=\begin{bmatrix}1&0&0&0&0&0&0&0\\0&1&0&0&0&0&0&0\\0&0&1&0&0&0&-1&0\\0&0&0&1&0&0&0&-1\\-1&0&S5&S6&1&0&0&0\\0&-1&S7&S8&0&1&0&0\\0&0&0&0&1&d&d^2&d^3\\0&0&0&0&0&1&2d&3d^2\end{bmatrix}$$

$$\mathbf{D}_\gamma=\begin{bmatrix}1&0&0&0\\0&1&0&-1\\-1&S9&1&0\\0&0&1&d\end{bmatrix},\quad \text{where } \begin{aligned}S1&=2c_{44}EI_zd_1, & S2&=6c_{44}EI_zd_1^2\\ S3&=-2c_{44}EI_z, & S4&=-6c_{44}EI_zd_1\\ S5&=2c_{55}EI_yd_1, & S6&=6c_{55}EI_yd_1^2\\ S7&=-2c_{55}EI_y, & S8&=-6c_{55}EI_yd_1\\ S9&=-c_{66}GJ\end{aligned} \tag{A.1}$$

$$\mathbf{P}=[1\ \ x\ \ x^2\ \ x^3],\quad \mathbf{R}=[1\ \ x]$$

$$\mathbf{a}_1=[a_1\ \ a_2\ \ a_3\ \ a_4]^{\mathrm{T}},\quad \mathbf{b}_1=[b_1\ \ b_2\ \ b_3\ \ b_4]^{\mathrm{T}},\quad \mathbf{c}_1=[c_1\ \ c_2]^{\mathrm{T}}$$

$$\mathbf{a}_2=[a_5\ \ a_6\ \ a_7\ \ a_8]^{\mathrm{T}},\quad \mathbf{b}_2=[b_5\ \ b_6\ \ b_7\ \ b_8]^{\mathrm{T}},\quad \mathbf{c}_2=[c_3\ \ c_4]^{\mathrm{T}} \tag{A.2}$$

References

[1] N. Challamel, Lateral-torsional buckling of beams under combined loading: a reappraisal of Papkovitch–Schaefer theorem, *International Journal of Structural Stability and Dynamics* 7 (2007) 55–79.
[2] S.P. Timoshenko, J.M. Gere, *Theory of Elastic Stability*, second ed., McGraw-Hill, New York, 1961.
[3] D.H. Hodges, D.A. Peters, On the lateral buckling of uniform slender cantilever beams, *International Journal of Solids and Structures* 11 (1975) 1269–1280.
[4] E. Reissner, Lateral buckling of beams, *Computers & Structures* 33 (1989) 1289–1306.
[5] D.H. Hodges, D.A. Peters, Lateral-torsional buckling of cantilevered elastically coupled composite strip- and I-beams, *International Journal of Solids and Structures* 11 (2001) 1585–1603.
[6] N. Challamel, A. Andrade, D. Camotim, An analytical study on the lateral-torsional buckling of linearly tapered cantilever strip beams, *International Journal of Structural Stability and Dynamics* 7 (2007) 441–456.
[7] L. Zhang, G.S. Tong, Elastic flexural-torsional buckling of thin-walled cantilevers, *Thin-Walled Structures* 46 (2008) 27–37.
[8] P. Mandal, C.R. Calladine, Lateral-torsional buckling of beams and the Southwell plot, *International Journal of Mechanical Sciences* 44 (2002) 2557–2571.
[9] M.M. Attard, Lateral buckling analysis of beams by the FEM, *Computers & Structures* 23 (1986) 217–231.
[10] H. Lee, D.-W. Jung, J.-H. Jeong, S. Im, Finite element analysis of lateral buckling for beam structures, *Computers & Structures* 53 (1994) 1357–1371.
[11] C. Karaagac, H. Öztürk, M. Sabuncu, Lateral dynamic stability analysis of cantilever laminated composite beam with an elastic support, *International Journal of Structural Stability and Dynamics* 7 (2007) 377–402.
[12] G.J. Turvey, Lateral buckling tests on rectangular cross-section pultruded GRP cantilever beams, *Composites: Part B* 27B (1996) 35–42.
[13] V. Thevendran, N.E. Shanmugam, Lateral buckling of narrow rectangular beams containing openings, *Computers & Structures* 43 (1992) 247–254.
[14] N.E. Shanmugam, V. Thevendran, Critical loads of thin-walled beams containing web openings, *Thin-Walled Structures* 14 (4) (1992) 291–305.
[15] M. Kisa, Free vibration analysis of a cantilever composite beam with multiple cracks, *Composites Science and Technology* 64 (2004) 1391–1402.
[16] A.D. Dimarogonas, Vibration of cracked structures: a state of the art review, *Engineering Fracture Mechanics* 55 (1996) 831–857.
[17] M.H.H. Shen, C. Pierre, Free vibration of beams with a single-edge crack, *Journal of Sound and Vibration* 170 (1994) 237–259.
[18] M. Krawczuk, W.M. Ostachowicz, Modelling and vibration analysis of a cantilever composite beam with a transverse open crack, *Journal of Sound and Vibration* 183 (1995) 69–89.
[19] G. Bamnios, A. Trochides, Dynamic behaviour of a cracked cantilever beam, *Applied Acoustics* 45 (1995) 97–112.
[20] T. Yokoyama, M.C. Chen, Vibration analysis of edge-cracked beams using a line-spring model, *Engineering Fracture Mechanics* 59 (1998) 403–409.
[21] T.D. Chaudhari, S.K. Maiti, Modelling of transverse vibration of beam of linearly variable depth with edge crack, *Engineering Fracture Mechanics* 63 (1999) 425–445.
[22] M. Krawczuk, A. Zak, W. Ostachowicz, Elastic beam finite element with a transverse elasto-plastic crack, *Finite Elements in Analysis and Design* 34 (2000) 61–73.
[23] S. Orhan, Analysis of free and forced vibration of a cracked cantilever beam, *NDT&E International* 40 (2007) 443–450.
[24] K. Wang, D.J. Inman, C.R. Farrar, Modelling and analysis of a cracked composite cantilever beam vibrating in coupled bending and torsion, *Journal of Sound and Vibration* 284 (2005) 23–49.
[25] G.L. Qian, S.-N. Gu, J.-S. Jiang, The dynamic behaviour and crack detection of beam with a crack, *Journal of Sound and Vibration* 138 (1990) 233–243.
[26] A. Gounaris, A. Dimarogonas, A finite element of a cracked prismatic beam for structural analysis, *Computers & Structures* 8 (1988) 309–313.
[27] T.G. Chondros, A.D. Dimarogonas, J. Yao, A continuous cracked beam vibration theory, *Journal of Sound and Vibration* 215 (1998) 17–34.
[28] P.N. Saavedra, L.A. Cuitino, Crack detection and vibration behavior of cracked beams, *Computers & Structures* 79 (2001) 1451–1459.
[29] A. Chajes, *Principles of Structural Stability Theory*, Prentice-Hall, Englewood Cliffs, NJ, 1974.

[30] H.P. Lee, T.Y. Ng, Natural frequencies and modes for the flexural vibration of a cracked beam, *Applied Acoustics* 42 (1994) 151–163.
[31] J. Fernandez-Saez, L. Rubio, C. Navarro, Approximate calculation of the fundamental frequency for bending vibrations of cracked beams, *Journal of Sound and Vibration* 225 (1999) 345–352.
[32] P. Gudmundson, The dynamic behaviour of slender structures with cross-sectional cracks, *Journal of the Mechanics and Physics of Solids* 31 (1983) 329–345.